4-2016

Differential Tilt Variance Effects of Turbulence in Imagery: Comparing Simulation with Theory

Daniel A. LeMaster
Air Force Research Laboratory

Russell C. Hardie
University of Dayton, rhardie1@udayton.edu

Szymon Gladysz
Fraunhofer Institute of Optronics, System Technologies and Image Exploitation

Matthew D. Howard
Air Force Research Laboratory

Michael Armand Rucci
Air Force Research Laboratory

See next page for additional authors

Differential tilt variance effects of turbulence in imagery: comparing simulation with theory

Daniel A. LeMaster*[a], Russell C. Hardie[b], Szymon Gladysz[c], Matthew D. Howard[a], Michael A. Rucci[a], Matthew E. Trippel[a], Jonathan D. Power[a], Barry K. Karch[a]
[a]Air Force Research Laboratory, 2241 Avionics Circle, Wright Patterson AFB, OH 45433;
[b]Department of Electrical and Computer Engineering, University of Dayton, 300 College Park, Dayton, Ohio 45459; [c]Fraunhofer Institute of Optronics, System Technologies and Image Exploitation, Gutleuthausstr. 1, 76275 Ettlingen, Germany

ABSTRACT

Differential tilt variance is a useful metric for interpreting the distorting effects of turbulence in incoherent imaging systems. In this paper, we compare the theoretical model of differential tilt variance to simulations. Simulation is based on a Monte Carlo wave optics approach with split step propagation. Results show that the simulation closely matches theory. The results also show that care must be taken when selecting a method to estimate tilts.

Keywords: Imaging, turbulence, tilt anisoplanatism, differential tilt, monte carlo, wave optics

1. INTRODUCTION

Differential Tilt Variance (DTV) is a measure of tilt anisoplanatism; it relates how apparent motion evolves spatially in a sequence of turbulence degraded images. For imaging scenarios where the sensor field-of-view subtends many isoplanatic patches, DTV can be used as an expression of requirements on dewarping for image restoration algorithms. Specifically, DTV could be used to compute the size of an isokinetic patch to be used as a block in these algorithms. Along with due consideration for higher order aberrations, DTV may also aid kernel size selection in lucky-region fusion[1] or for the processing block size used in bispectrum speckle techniques[2]. Furthermore, we hope to use DTV to improve predictive models of image quality that, at present, do not account for anisoplanatism.

DTV for spherical wave propagation was derived and verified experimentally over horizontal paths by Gladysz et al[3]. Using an array of Light Emitting Diode (LED) point sources and this model of DTV, they were able to infer refractive index structure constant, outer scale and the slope of the turbulence power spectrum. In this paper, we compare theory to an anisoplanatic turbulence simulator that recreates conditions of the Gladysz field collect. This comparison is of general interest because differential tilt variance is not factored explicitly into simulation design (specifically, into phase screen selection) yet it is a readily identifiable effect in imagery and easily measurable, as opposed to higher-order aberrations for which a wavefront sensor is needed.

The Monte-Carlo wave optics turbulence simulator used in this paper is based on the well-known split-step approach where radiation propagates from object space, through a series of turbulence phase screens, and into the receiving aperture using the Fresnel/angular spectrum method. This particular implementation draws on two sources from the literature[4-5]. Specifically, unique turbulence degraded Point Spread Functions (PSFs) are calculated and applied to each point in the true object image in order to simulate the space-varying effects of turbulence. This approach is one of several variations on wave-optics based methods. For instance, in another variation, a field corresponding to the entire object with a random realization of surface roughness is split-step propagated though a series of phase screens under frozen turbulence conditions. This process is repeated many times for different object surface phase realizations and averaged to produce a final incoherent image[6]. All other conditions being equal, simulation time for the technique used in this paper will be faster than the random surface roughness approach.

Turbulence simulators are a useful way to evaluate image restoration performance; therefore, it is necessary to verify that the differential tilt variance predicted by theory is observed in the simulated results. Background on differential tilt variance is presented in Section 2. The experiment and results are presented in Section 3. This paper concludes with interpretation and conclusions in Section 4.

Long-Range Imaging, edited by Eric J. Kelmelis, Proc. of SPIE Vol. 9846 984606
 · doi: 10.1117/12.2223470

2. DIFFERENTIAL TILT VARIANCE

Images formed through volume turbulence suffer from space-varying blur and distortions. The apparent displacement of points in an image from their true object position is referred to as tilt. Images exhibit statistical similarity in tilt over relatively large regions compared to the isoplanatic patch. Differential tilt variance is a structure function that describes the statistical relationship between observed tilts as a function of separation distance.

2.1 Theory

Gladysz et al. provides a general theoretical expression for different tilt variance[3]. This expression includes parameterization for turbulence strength, C_n^2, outer scale, L_0, slope of the power spectrum, α, and anisotropy in any of these terms. Our simulations attempt to approximate Kolmogorov conditions (i.e. very large outer scale, 11/3 power spectrum slope, and no anisotropy) with constant C_n^2. These conditions correspond to an observable differential tilt variance that is prescribed by theory. The theoretical expression for differential tilt variance between two points separated by distance, d, in the direction along their common axis (σ_c^2) and perpendicular to it (σ_p^2) is given by:

$$\begin{bmatrix}\sigma_c^2\\ \sigma_p^2\end{bmatrix} = \frac{6.6336}{D^2} A(\alpha)\tilde{C}_n^2 \int_0^R dz \int d\underline{\kappa} \begin{bmatrix}\cos^2\varphi\\ \sin^2\varphi\end{bmatrix} \left(\kappa^2 + \left(\frac{2\pi}{L_o}\right)^2\right)^{-\alpha} J_1^2\left(\frac{z\kappa D}{2R}\right)\left(1-\cos\left(\kappa d\cos\varphi\right)\right) \quad (1)$$

with D as the imaging system's entrance pupil diameter, R is the length of the path from object to imager, and $\underline{\kappa}$ is two-dimensional spatial frequency composed of magnitude κ and angle φ. $A(\alpha)$ and the $\sim$ over the C_n^2 term are used to represent a generalized definition of turbulence strength when the slope of the power spectrum is something other than *11/6*. Note that this value is 11/6, and not the standard Kolmogorov value of 11/3, because κ is squared within the term containing the outer scale. When α=*11/6* and *A(α)* is unity, C_n^2 is restored to its conventional definition. Note that, unlike the isoplanatic angle, DTV is *not* wavelength dependent.

2.2 Estimation techniques

DTV is appealing as an expression of turbulent distortion because, in measurement, it is insensitive to small defocus errors and global translational motion, e.g. from vibrations, thermal drifts or panning. Additionally, estimation of differential tilt variance from imagery is conceptually straightforward. As an example, the geometry of differential tilt variance along an axis that runs through two point sources separated by distance, d, is shown in Figure 1.

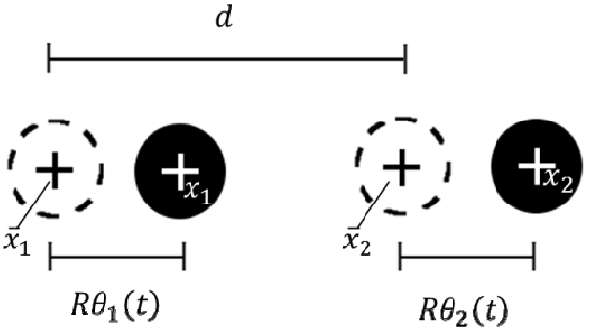

Figure 1. Differential tilt variance along the axis common to two point sources in object space coordinates. The dashed circles show the true location of the sources while the solid circles show the apparent tilt positions at time *t*.

An estimate of differential tilt variance for this scenario is given by:

$$\sigma_c^2 = \left\langle \left[\theta_1(t) - \theta_2(t)\right]^2 \right\rangle = \frac{1}{R^2}\left\langle \left[\left(x_1(t) - \langle x_1(t)\rangle\right) - \left(x_2(t) - \langle x_2(t)\rangle\right)\right]^2 \right\rangle, \quad (2)$$

where θ_1 and θ_2 are the observed tilts of each point in angular units at time t, x_1 and x_2 are the observed tilts in object space, and the outer brackets, ⟨ ⟩, denote the time average over many observations. Equation 2 is rearranged so that,

$$\sigma_c^2 = \frac{1}{R^2}\left\langle \left[\left(x_1(t) - x_2(t)\right) - \left(\left\langle x_1(t)\right\rangle - \left\langle x_2(t)\right\rangle\right) \right]^2 \right\rangle . \quad (3)$$

Recalling that, in all cases[8], $\left\langle x_1(t)\right\rangle - \left\langle x_2(t)\right\rangle = \left\langle x_1(t) - x_2(t)\right\rangle$, Equation 3 shows that the estimate of differential tilt variance follows directly from the variance of the difference in observed tilts. It is straightforward to derive an identical result for the σ_p^2 case. Regression can be used to fit estimates of σ_p^2 and σ_c^2 from imagery to values of turbulence strength, spectral slope, and outer scale via Equation 1. The requirement for accurate tilt estimation is implicit in Equation 3. Three tilt estimation techniques were applied in this paper, two based on centroiding and a third based on template matching in Fourier space.

The first centroiding process utilizes a multipass algorithm to separate each LED object in the frame and then calculate the location of the centroid. The first pass begins by thresholding to determine a region of interest around each LED. Next, the objects are detected from the mask by using the OpenCV contour finding routine and considering the largest contours to correspond to the objects. The central moments of the contours are used to obtain estimated centroids for the two objects. The second pass takes the estimated centroids and uses the region around them to find the power-weighted centroid of each object.

In the second centroiding process, regions containing LED signals are determined by thresholding the image above three standard deviations of the noise floor after local background subtraction. The noise floor is also estimated from the imagery. Pixels containing signal above this threshold are then used to find the centroid for each LED.

For the template matching tilt estimator, an idealized reference image is cross-correlated in Fourier space with the measured signal. In the discrete Fourier transform domain, both the reference and measured data are upsampled by a factor of 10 using zero-padding. The idealized reference image for each individual LED is determined from the average image over the collected sequence. In field collections, this is an important consideration for imaging over short distances because the experimental LEDs are slightly resolved and each looks a bit different. In simulation, the LEDs are closer to true points. This is the tilt estimator used during field trials[3].

3. ANALYSIS OF SIMULATED RESULTS

Our simulation attempts to recreate the conditions of the experiment at the Institute of Saint-Louis (ISL) discussed in reference [3] (specifically, Figure 2). The experiment included a 10 by 10 array of white light LEDs, spaced 5 cm apart, and imaged from a range of 270 m. The telescope used in this experiment had an aperture diameter of 145 mm, focal length is 800 mm, and detector pitch of 5.5 μm. DTV estimates were extracted from 1000 frames of short exposure imagery collected at 100 Hz. Turbulence strength is $4.2\text{x}10^{-14}$ $m^{-2/3}$ along the path as measured by a scintillometer. For the purposes of simulation, the LEDs are assumed to be point sources with 600 nm wavelength. Also, we simulated a 13 by 13 LED array (rather than a 10 by 10).

3.1 Simulation parameters

Our Monte-Carlo wave optics simulation technique was discussed in Section 1. To significantly speed up processing, each LED image is calculated separately and stitched together to form the composite array. This is an effective approach because each LED image is essentially a short exposure point spread function on a black background. Volume turbulence is approximated using two phase screens, evenly spaced along the path (i.e. at 90 m and 180 m), and scaled based on a variation of the Bos and Roggemann method[5]. The phase screens are selected to match the theoretical coherence diameter but the discrete isoplanatic angle was scaled down so that the empirical isoplanatic angle was a better match with the theoretical after generating images. Agreement with theoretical log amplitude variance is deemphasized since each point spread function is assigned equal amplitude. The phase screens are generated using the von Karman power spectrum with 3 levels of subharmonics. Table 1 summarizes the details of the simulation and Figure 3 shows 3 by 3 LED image chips extracted from three successive frames. The chips have been upsampled and contrast stretched to aid visualization.

Table 1. A summary of simulation conditions.

	theoretical	discrete	units
coherence diameter	4.2	4.2	cm
isoplanatic angle	49	40	μrad
log amplitude variance	0.023	0.04	unitless

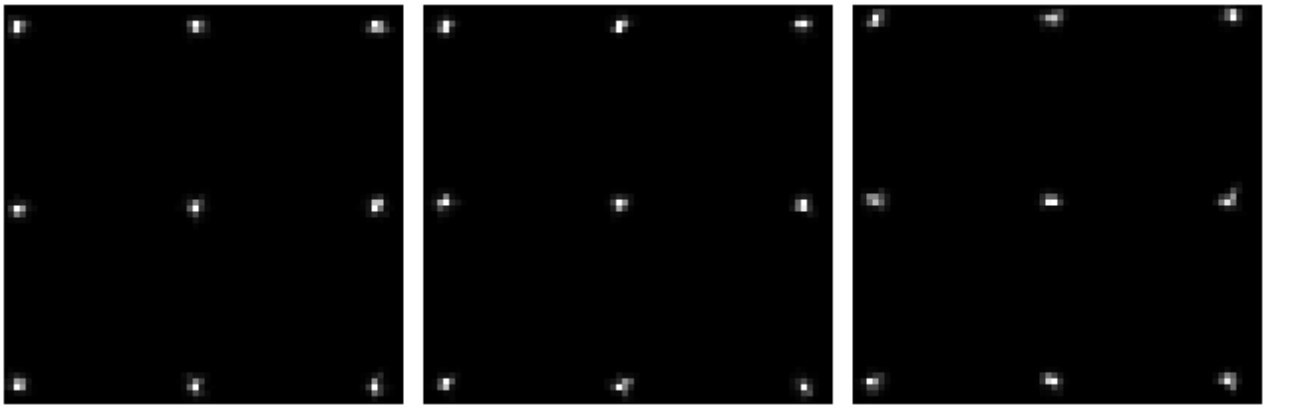

Figure 3. 3 x 3 LED array images in turbulence as simulated with the Monte-Carlo approach (upsampled and contrast stretched).

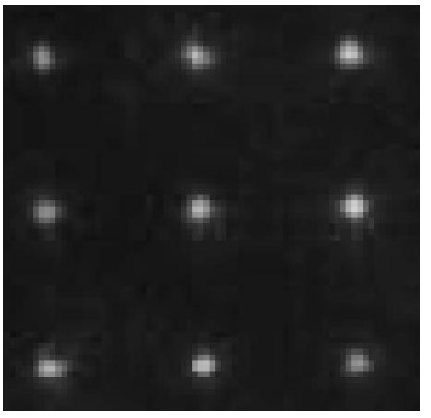

Figure 4. 3 x 3 LED array sample from the field collection in [3].

Figure 4 shows a 3 by 3 LED region extracted from an image taken during the field collect[3]. It is visibly softer than the simulated data. Several factors may contribute to this difference: the real LEDs were not true point sources; real LEDs are polychromatic; the simulation does not include the true telescope and detector array modulation transfer characteristics; and, perhaps most importantly, it is easy to achieve perfect focus in simulation but difficult to do so for turbulence degraded imagery in practice. Our assumption is that the unmodeled effects contributing to blur do not degrade the apparent motion that is key to estimating differential tilt variance.

3.2 Comparing simulation and theory

Figure 5 summarizes how differential tilt variance estimates are affected by choice of tilt estimator. Each estimate includes all possible tip (x) and tilt (y) combinations of LED separations, e.g. 312 estimates for 5 cm spacing at each DTV orientation, 286 estimates for 10 cm spacing, et cetera. It is clear that the Fourier cross-correlation estimator provides results that are most in agreement with the theoretical values overall. Centroid method 2 slightly outperforms

the Fourier method when only the perpendicular case (σ_p^2) is considered. As a useful point of comparison, the field trial results from Figure 2 in reference 3, which is precisely the case that we attempted to simulate, are also included in the plot.

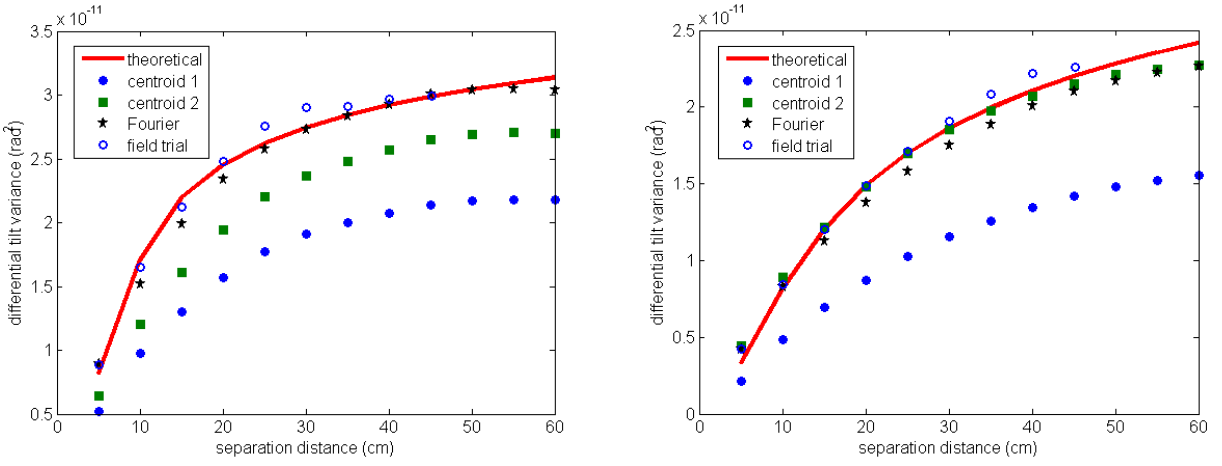

Figure 5. A comparison of Differential Tilt Variance theory and simulations.
(Left) Parallel to the common axis between sources. (Right) Perpendicular to the common axis between sources.

The close agreement between the Fourier method and theory was anticipated as this is also the standard model used by the authors of the field trial. Taken on its face, this result seems to show that the Monte-Carlo wave optics simulation does give rise to the correct differential tilt variance statistics even though this measure is not considered explicitly when selecting the location and composition of the phase screens.

It is instructive to consider the results in Figure 5 in terms of the C_n^2 values that best fit the estimated DTV curves. Best fit is defined to be in the minimum mean squared error sense. Table 2 contains multiple different estimates of C_n^2 across the three tilt estimators. C_n^2 is estimated for the parallel and perpendicular variances for both the horizontal (along each row of LEDs) and vertical (along each column of LEDs) directions in all possible combinations. At the bottom of Table 2, these results are recast in terms of percent deviation from the theoretical value, 4.2×10^{-14} $m^{-2/3}$. Outer scale estimates were all much larger than 10 m. Consequently, there is no significant deviation in these results when outer scale is assumed to be infinite.

Table 2. Turbulence strength estimates from each tilt estimator for all orientation combinations.

C_n^2 ($\times 10^{-14}$)	horizontal			vertical			horizontal and vertical together		
	parallel	perpendicular	combined	parallel	perpendicular	combined	parallel	perpendicular	combined
Centroid 1	3.04	2.59	2.89	2.76	2.72	2.72	2.89	2.65	2.83
Centroid 2	3.75	3.39	3.63	3.4	4.85	3.87	3.6	4.12	3.73
Fourier	4.32	4.08	4.23	3.92	3.91	3.93	4.12	4.01	4.06

C_n^2 error (%)	horizontal			vertical			horizontal and vertical together		
	parallel	perpendicular	combined	parallel	perpendicular	combined	parallel	perpendicular	combined
Centroid 1	-27.6	-38.3	-31.2	-34.3	-35.2	-35.2	-31.2	-36.9	-32.6
Centroid 2	-10.7	-19.3	-13.6	-19.0	15.5	-7.9	-14.3	-1.9	-11.2
Fourier	2.9	-2.9	0.7	-6.7	-6.9	-6.4	-1.9	-4.5	-3.3

Table 2 confirms the agreement between theory and the simulated data when the Fourier estimator is used. C_n^2 estimates tend to fall below the theoretical value (if only slightly in the Fourier case). More experimentation is required to determine if this discrepancy can be traced to the tilt estimators or to the simulation. Ideally, there would be perfect agreement between the theory and the model. That being said, it is worth mentioning that the variation in C_n^2 estimates is equivalent to or smaller than variation seen in field measurements of C_n^2 using scintillometers. There is no definitive evidence of anisotropy when comparing the C_n^2 estimates across the horizontal and vertical cases. Results from the Centroid 1 and Fourier estimators are slightly higher in the horizontal case while, for Centroid 2, the vertical case is slightly higher. Neither parallel nor perpendicular fits show any strong advantage over the others in terms of percent error. Out of all possible variations, it is clear that choice of tilt estimator has the most demonstrable impact on performance.

4. CONCLUSION

We intend to use differential tilt variance as a means to discuss and compare the effects of anisoplanatism across different turbulence restoration algorithms, approaches to turbulence mitigation, and image quality performance models. Differential tilt variance is useful for these tasks because it describes (in a statistical sense) how turbulence induced apparent motion in imagery evolves over angles that are much larger than the isoplanatic patch. We expect this measure to be particularly salient in the evaluation of algorithms that depend on space-varying block or kernel processing.

In this paper, we simulated turbulence degraded imagery of an LED array with conditions corresponding to a recent field collect where differential tilt variance was used to estimate C_n^2, outer scale, and the slope of the turbulence power spectrum. The turbulence simulation used in the paper employs a wave optics Monte Carlo approach with split step propagation where phase screen placement and properties are selected to closely match the coherence diameter and isoplanatic angle of the bulk turbulence. Consequently, our initial hypothesis was that simulated differential tilt variance would make a poor comparison to theory because differential tilt variance is not considered explicitly in the phase screen selection process. After processing the results, we have determined that this hypothesis was incorrect; in fact, theory and simulation are in good agreement when tilts are estimated using the approach recommended from the field collect campaign.

ACKNOWLEDGEMENTS

A significant portion of this analysis is based upon work supported by the Air Force Office of Scientific Research, Air Force Material Command, USAF under Award No. FA9550-14-1-0244. The turbulence simulator used in this effort was developed under funding from L-3 / Cincinnati Electronics.

REFERENCES

[1] Aubailly M., Vorontsov M.A., Carhart G.W., Valley M.T., “Automated video enhancement from a stream of atmospherically-distorted images: the lucky-region fusion approach,” Proc. SPIE 7463, (2009).
[2] Curt, P. F., Bodnar, M. R., Ortiz, F. E., Carrano, C. J., & Kelmelis, E. J., “Real-time embedded atmospheric compensation for long-range imaging using the average bispectrum speckle method,” Proc. SPIE 7244, (2009).
[3] Gladysz, S., Segel, M., Eisele, C., Barros, R., & Sucher, E.,” Estimation of turbulence strength, anisotropy, outer scale and spectral slope from an LED array,” Proc. SPIE 9614 (2015).
[4] Schmidt, J. D., [Numerical simulation of optical wave propagation with examples in MATLAB], SPIE, Washington, (2010)
[5] Bos, J.P., Roggemann, M.C., “Technique for simulating anisoplanatic image formation over long horizontal paths,” Optical Engineering 51(1), (2012).
[6] Underwood, T.A., Voelz, D.G., “Wave optics approach for incoherent imaging simulation through distributed turbulence,” Proc. SPIE 8877, (2013).
[7] Lachinova, S. L., Vorontsov, M. A., Dudorov, V. V., Kolosov, V. V., & Valley, M. T., “"Anisoplanatic imaging through atmospheric turbulence: Brightness function approach," Proc. SPIE 6708, (2007).
[8] Leon-Garcia, A., [Probability and Random Processes for Electrical Engineering 2nd ed], Addison Wesley Longman, Reading MA (1994)